J Solid State Electrochem (2008) 12:815–823
DOI 10.1007/s10008-007-0498-7

ORIGINAL PAPER

Physical and electrochemical properties of La-doped $LiFePO_4$/C composites as cathode materials for lithium-ion batteries

Yung-Da Cho · George Ting-Kuo Fey · Hsien-Ming Kao

Received: 1 July 2007 / Revised: 3 December 2007 / Accepted: 7 December 2007 / Published online: 15 March 2008

Abstract Olivine-type $LiFePO_4$ is one of the most promising cathode materials for lithium-ion batteries, but its poor conductivity and low lithium-ion diffusion limit its practical application. The electronic conductivity of $LiFePO_4$ can be improved by carbon coating and metal doping. A small amount of La-ion was added via ball milling by a solid-state reaction method. The samples were characterized by X-ray diffractometer (XRD), scanning electron microscopy (SEM)/mapping, differential scanning calorimetry (DSC), transmission electron microscopy (TEM)/energy dispersive X-ray spectroscopy (EDS), and total organic carbon (TOC). Their electrochemical properties were investigated by cyclic voltammetry, four-point probe conductivity measurements, and galvanostatic charge and discharge tests. The results indicate that these La-ion dopants do not affect the structure of the material but considerably improve its rate capacity performance and cyclic stability. Among the materials, the $LiFe_{0.99}La_{0.01}PO_4$/C composite presents the best electrochemical behavior, with a discharge capacity of 156 mAh g^{-1} between 2.8 and 4.0 V at a 0.2 C-rate compared to 104 mAh g^{-1} for undoped $LiFePO_4$. Its capacity retention is 80% after 497 cycles for $LiFe_{0.99}La_{0.01}PO_4$/C samples. Such a significant improvement in electrochemical performance should be partly related to the enhanced electronic conductivities (from 5.88×10^{-6} to 2.82×10^{-3} S cm^{-1}) and probably the mobility of Li^+ ion in the doped samples. The $LiFe_{0.99}La_{0.01}PO_4$/C composite developed here could be used as a cathode material for lithium-ion batteries.

Keywords Lanthanum doping · $LiFePO_4$ · Carbon · Cathode · Li-ion batteries

Contribution to ICMAT 2007, Symposium K: Nanostructural and bulk materials for electrochemical power sources, July 1–6, 2007, Singapore

Y.-D. Cho · G. T.-K. Fey (✉)
Department of Chemical and Materials Engineering,
National Central University,
Chung-Li, Taiwan 32054, People's Republic of China
e-mail: gfey@cc.ncu.edu.tw

H.-M. Kao
Department of Chemistry, National Central University,
Chung-Li, Taiwan 32054, People's Republic of China

Introduction

The increasing demand for portable consumer electronic has driven the successful development of advanced lithium-ion batteries with high energy density and long cycle life. Currently, $LiCoO_2$ is the most widely used cathode material in commercial lithium-ion batteries [1–3], but it is limited to small-rate 3C applications due to safety concerns. Recently, $LiFePO_4$, which was discovered by Goodenough et al. in 1997 [4], has emerged as a new cathode material. This material has the advantages of being nontoxic, inexpensive, and environmentally friendly. Furthermore, it has a high theoretical specific capacity (170 mAh g^{-1}), proper charge–discharge voltage (about 3.5 V vs Li/Li^+), excellent thermal stability, and good cycling performance. In particular, $LiFePO_4$ has been considered as an ideal high-power cathode material for large-size lithium-ion batteries in applications related to electric vehicles (EVs) and hybrid electric vehicles (HEVs).

However, $LiFePO_4$ suffers from low rate capacity due to its poor conductivity and low Li^+ diffusion kinetics. Ways to overcome the above limitations may involve the use of lattice and non-lattice doping methods. The latter method includes coating particles with carbon [5–9] or co-synthesizing the compounds with silver or copper metal powders [10], and these dopants act as conductivity bridges or

nucleation sites for the formation of $LiFePO_4$ crystals [5–10]. Many attempts have been made to enhance the electronic conductivity and electrochemical properties of $LiFePO_4$ materials through different synthesis techniques. Nano-size $LiFePO_4$ powders have been synthesized by using partially oxidized carbon particles as a nucleating agent [11–13]. These nano-size materials have achieved 90% theoretical capacity at a moderate current rate, because the small and uniform size of the $LiFePO_4$ particles may shorten the Li^+ diffusion path and improve electrochemical properties. The conductivity of $LiFePO_4$ can be improved by dispersing copper /silver powders [10, 14–15] or high surface area carbon black [16], and coating with carbon [5–8, 17–18] to provide pathways for electron transference. Furthermore, supervalent elements [19–23] are also available as dopant materials.

In this paper, we combined the above two methods, and synthesized $LiFe_{1-x}La_xPO_4/C$ composite materials through lattice doping with La^{3+} cation and non-lattice doping with carbon. The conductivity of $LiFePO_4$ was enhanced significantly via carbon coating and La doping. The physical, structural, and electrochemical properties of $LiFe_{1-x}La_xPO_4/C$ composites were systematically investigated.

Experimental

The pure and doped composite $LiFePO_4$ samples were synthesized via a solid-state method. The starting material Li_2CO_3 (99%, Aldrich), $FeC_2O_4{\cdot}2H_2O$ (98.5%, Aldrich), $La(NO_3)_3{\cdot}6H_2O$ (99%, Aldrich), and $(NH_4)_2HPO_4$ (98.5%, Aldrich) were mixed in atomic ratio of Li: (Fe + La): PO_4= 1:1:1. The mixtures were milled in an inert atmosphere to avoid the oxidation of Fe^{2+} to Fe^{3+} in a planet mixer for 3 h. After milling, the mixtures were calcined in a tube furnace at 593 K for 10 h under 5% H_2 in an argon atmosphere to decompose the starting salts. The resulting precursor was mixed with salicylic acid in acetone, and ball-milled under argon for 30 min. Finally, the mixture was further calcined at 873 K under a flowing gas mixture (5% H_2 in Ar). A reducing atmosphere was employed during the calcination process to avoid the oxidation of Fe^{2+} cations.

An X-ray diffractometer (XRD), Siemens D-5000, Mac Science MXP18, equipped with a nickel-filtered Cu-K_α radiation source (λ=1.5405 Å) was used for structural analysis. The diffraction patterns were recorded between scattering angles of 15° and 80° in steps of 4°. The surface morphology of the coated materials was studied using a scanning electron microscope (SEM), Hitachi model S-3500N, equipped with a Noran instruments (455A-1SPS) for energy dispersive spectroscopy (EDS). The microstructure and lattice images of the coated particles were observed with a high-resolution transmission electron microscope (HRTEM, Hitachi HF 2000) equipped with a LaB_6 gun. Electron diffraction patterns were obtained through selected area electron diffraction (SAED). The chemical composition of the separated phases was determined by nanobeam energy dispersive spectroscopy (EDS). For these experiments, samples were previously dispersed in acetone and deposited on a holey silicon grid.

Carbon content analyses of the products were investigated on a OIA Model Solids module for the total organic carbon (TOC) analyzer apparatus with an oxygen gas rate of 40 kgf cm^{-2}. Raman spectroscopy was performed on samples of powders using a ISA T64000 double beam pass spectrometer equipped with a microscope stage for analyzing small samples utilizing 180° incident geometry. A Spectra Physics argon-ion laser was employed to excite laser Raman spectra using a 515-nm laser line at an incident power of ca. 10 mW along with a water-cooled photomultiplier tube. The scanning rate used to collect the spectra was kept at 10 $cm^{-1}min^{-1}$. The electronic conductivity of samples was measured by four-point conductivity measurements of Keithley Model 2400S source meter.

Experimental test cells for measurements used the cathode with a composition of 85 wt% active material, 10 wt% conductive carbon black, and 5 wt% poly (vinylidene fluoride) in *N*-methyl-2-pyrrolidone (NMP), as the solvent for the mixture, which was then applied onto an etched aluminum foil current collector and dried at 393 K for 3 h in an oven. The separator used was a Celguard 3501 microporous polypropylene membrane. The electrolyte was 1 M $LiPF_6$ in ethylene carbonate/diethyl carbonate EC:DEC (1:1 *v*/*v*) (Tomiyama Chemicals). A lithium metal (Foote Mineral) anode was used in this study. The cells were assembled in a glove box filled with argon gas. The charge/discharge cycling was galvanostatically performed at a current of 0.2 C-rate with cut-off voltages of 2.8 and 4.0 V (vs Li/Li^+) at 298 K in a multichannel battery tester (Maccor 4000).

Phase transitions occurring during the cycling processes were examined by slow scan cyclic voltammetry, performed with a three-electrode glass cell. The working electrodes were prepared with the cathode powders as described above and lithium metal foil serving as both counter and reference electrodes. The electrolyte used was the same as that for the coin cell. Cyclic voltammograms were run on a Solartron 1287 Electrochemical Interface at a scan rate of 0.1 mV s^{-1} between 3.0 and 4.0 V.

Results and discussion

XRD

The XRD patterns of pure $LiFePO_4$ and $LiFe_{0.99}La_{0.01}PO_4/C$ are shown in Fig. 1. All diffraction lines were in-

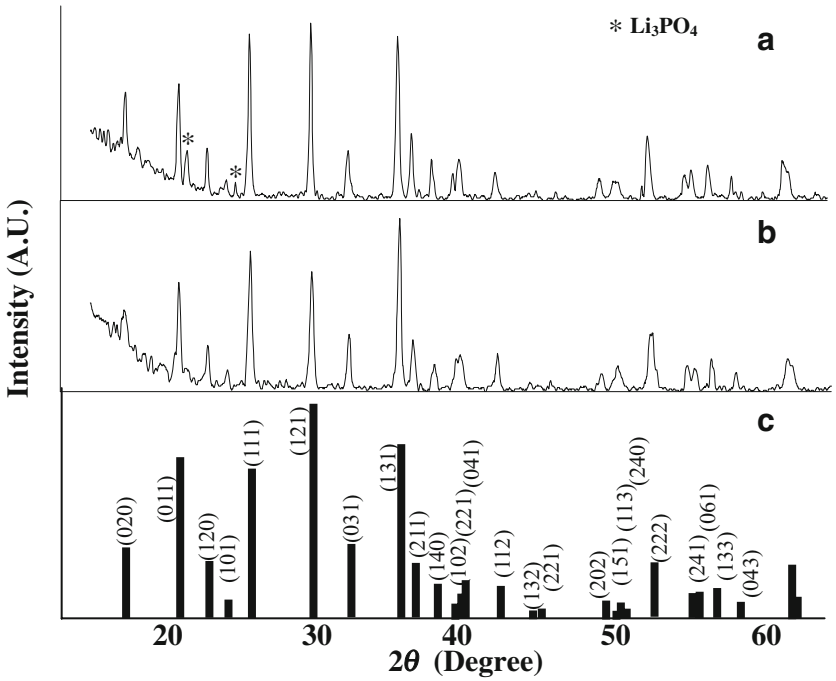

Fig. 1 X-ray diffraction patterns of **a** pure $LiFePO_4$; **b** $LiFe_{0.99}La_{0.01}PO_4$ /C; **c** JCPDS nos. 40–1,499 $LiFePO_4$

dexed to an orthorhombic crystal structure (space group P_{mnb}, triphylite). However, two peaks at 2θ =22.3° and 24.8° (marked with stars) are observed in pure $LiFePO_4$, which correspond to the impurity peaks of Li_3PO_4. From Fig. 1b, no phase impurities were detected on the $LiFe_{0.99}La_{0.01}PO_4$/C sample. A previous report found the impurity Li_3PO_4 in doped-$LiM_xFe_{1-2x}PO_4$ prepared by a solid-state method, even with a very low dopant level [24]. From the results of Herle et al. [25], the Ti-doped sample contains Li_3PO_4, Fe_3P, and $Fe_3(PO_4)_2$ as impurity phases, which are the same as those usually reported as impurities in aliovalent-doped $LiFePO_4$ samples. The crystallite size was calculated using the Scherrer's equation based on the half width of the (020) reflection [26]. The crystallite sizes of pure $LiFePO_4$ and $LiFe_{0.99}La_{0.01}PO_4$/C were 310 and 140 Å, respectively. In addition, it has been known that adding carbon restrains particle growth during longer calcinations [27].

DSC

The thermal stability of charged $LiFePO_4$ and $LiFe_{0.99}La_{0.01}PO_4$/C cathodes under controlled conditions was studied by DSC. Figure 2 shows the DSC results for 4.5 V charged $LiFePO_4$ and $LiFe_{0.99}La_{0.01}PO_4$/C composite cathodes in an argon atmosphere at a heating rate of 10 K min^{-1}. For $LiFePO_4$, exothermic heat flow was detected under a wide temperature range of 373 to 673 K, with total heat evolution of about 109.41 J g^{-1}. For the optimized composition of $LiFe_{0.99}La_{0.01}PO_4$/C, the total heat evolution was about 78.9 J g^{-1}. From these thermal data, it is clear that

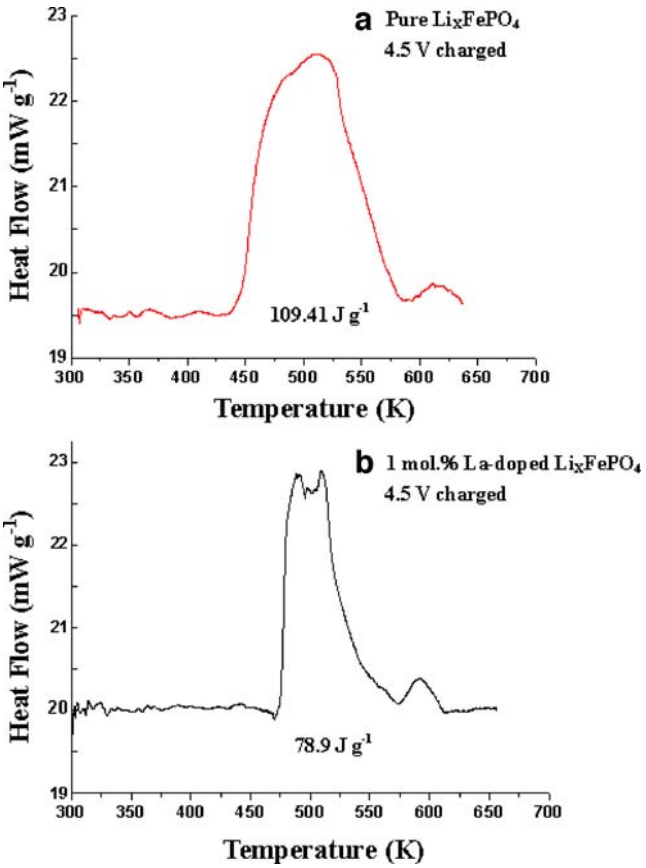

Fig. 2 DSC profiles of **a** pure $LiFePO_4$; **b** 1.0 mol% La-doped Li_XFePO_4/C. Charged to 4.5 V

exothermic heat flow can be reduced further by carbon coating and metal doping. Moreover, the onset temperature can be raised from 398 to 483 K. In contrast, charged $LiNiO_2$ and $LiCoO_2$ showed much greater heat evolution with significant oxygen loss [28]. For instance, the overall heat generation of the fully charged $LiNiO_2$ and $LiCoO_2$ were about 1,600 and 1,000 J g^{-1}, respectively. The excellent safety performance of the olivine structure could allow lithium-ion batteries to move beyond the traditional low-rate markets to high-rate robust systems. This exceptional thermal stability is attributed to the unique anion bonding and stability of phosphate materials with its shorter P–O bond and more tightly bound oxygen.

Morphology

During the ball-milling of starting materials for the preparation of $LiFe_{0.99}La_{0.01}PO_4/C$ composites, the salts containing Li^+, Fe^{2+}, La^{3+}, and PO_4^{3-} ions, as well as carbonaceous material were mixed well. We achieved elemental mapping of $LiFe_{0.99}La_{0.01}PO_4/C$ particles by energy dispersive spectroscopy. The elemental mapping of P, Fe, La, C, and O in $LiFe_{0.99}La_{0.01}PO_4/C$ samples are shown in Fig. 3a. A homogeneous distribution of the Fe, P, O, and C elements was observed in $LiFe_{0.99}La_{0.01}PO_4/C$ structure with a uniform distribution of the La-dopant element on the surface of the individual crystals.

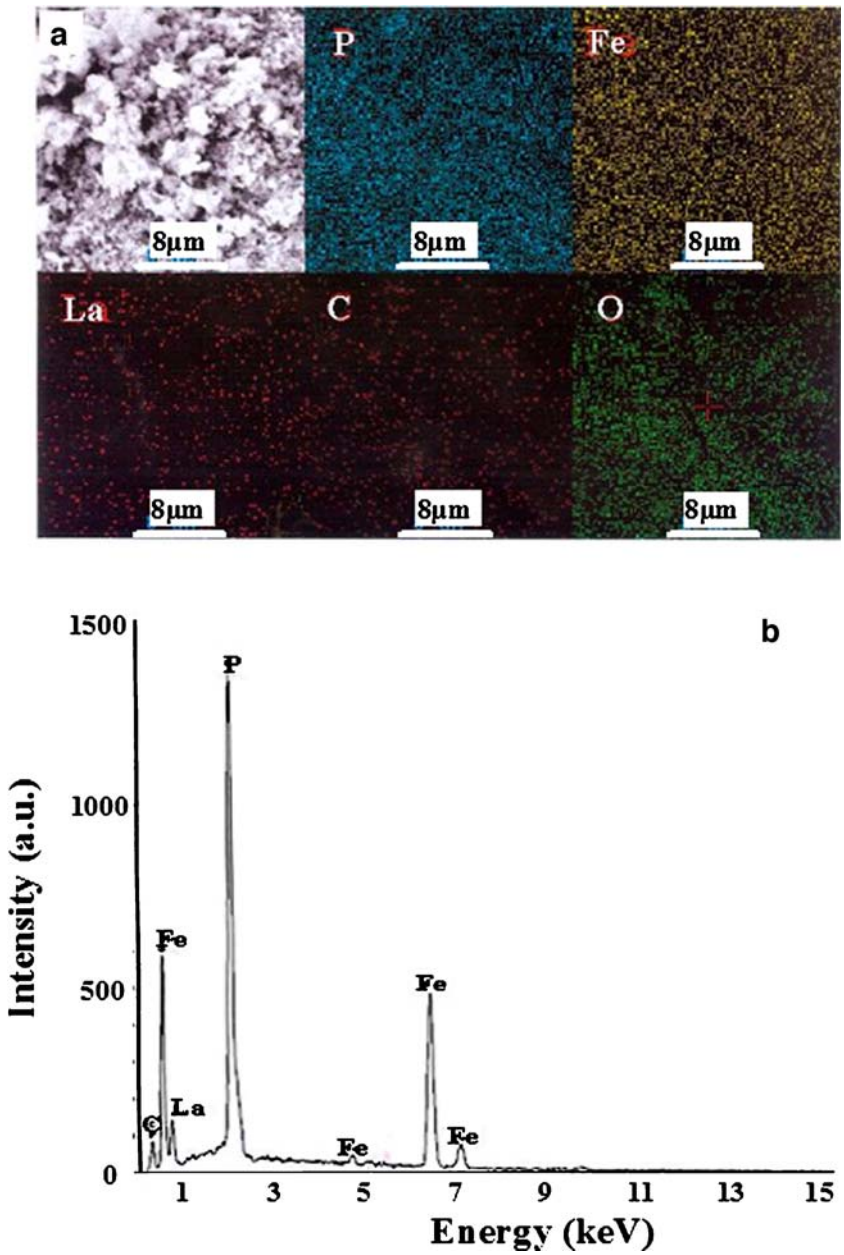

Fig. 3 **a** SEM micrograph and elemental mapping; **b** EDS of $LiFe_{0.99}La_{0.01}PO_4/C$ powders

To improve our understanding of the morphology on a nanostructural level, we conducted HRTEM analysis of $LiFe_{0.99}La_{0.01}PO_4/C$ particles in combination with SAED and EDS. The results are shown in Fig. 4. Figure 4a shows a TEM image of $LiFe_{0.99}La_{0.01}PO_4/C$ particles, which had a uniform coating about 50 nm in thick (Fig. 4b), although the composite particles were aggregated to form grains several hundred nanometers in size. The small particle size allows easy penetration of the electrolyte and provides a short pathway for Li^+ diffusion in the active material crystals. During heat treatment, salicylic acid was decomposed in an inert atmosphere and became a solid carbonaceous material. EDS analysis confirmed that the transparent layers are a carbon component (Fig. 4c), and the dark area includes Fe, P, O, La, and C components (Fig. 4d). We used SAED in combination with TEM. Figure 4e shows a hollow ring pattern typical for amorphous carbon in the outer layer, and the dark area exhibits a bright spot pattern in the core that is typical for crystalline $LiFePO_4$ as displayed in Fig. 4f. Thus, amorphous carbon films were clearly identified on the outer surface of $LiFe_{0.99}La_{0.01}PO_4/C$. Theories about the conduction mechanism of carbon coating and supervalent doping have been expanded in recent years. Chung et al. [20] and Ravet et al. [29] brought attention to the electron conduction and cycling performance of doped $LiFePO_4$ material. These authors have purported that conductivity can be enhanced because of heterogeneous doping and carbon presence. In addition, Herle et al. [19] have pointed to the presence of small amounts of phosphides or phosphocarbides, which were known for their metallic-like conducting properties.

The carbon content was determined by total organic carbon (TOC) analysis. Both pure and doped $LiFePO_4$ were pressed into disk-shaped pellets, and their electronic conductivities were measured by the four-point dc method. All pellets exhibited high electronic conductivity of 10^{-3}~10^{-4} S cm^{-1} at 300 K. If the carbon content was between 2.04 and 3.04 wt%, conductivity increased at higher La-dopant levels. As shown in Table 1, conductivity increased along with the carbon content of samples. The individual La-doped $LiFePO_4$ crystals were wired together by the coated carbon layer. The doping element induces p-type semiconductivity, and the carbon layer provides a conductive network. Therefore, it is not surprising that the combination of carbon coating and La-doping on the $LiFePO_4$ crystals could dramatically increase conductivity of the material and improve its electrochemical properties [24].

Raman spectroscopy

The structure of the deposited carbon on the surface of $LiFe_{0.99}La_{0.01}PO_4$ particles was investigated using Raman spectroscopy. Figure 5 and Table 2 display the Raman spectra of the $LiFe_{0.99}La_{0.01}PO_4/C$ composite obtained at various temperatures in the range of 700~1,700 cm^{-1}. In all cases, the spectra had a relatively small band at 950 cm^{-1} corresponding to the symmetric PO_4^{3-} stretching vibration in $LiFePO_4$ olivine structure [30]. The broad bands at 1,350 and 1,590 cm^{-1} are well known from the spectroscopy of carbon as being the D (sp^3-type) and G band (sp^2-type) that originate from amorphous and graphitic forms, respectively. Doeff et al. [31, 32] pointed out that the increasing amount

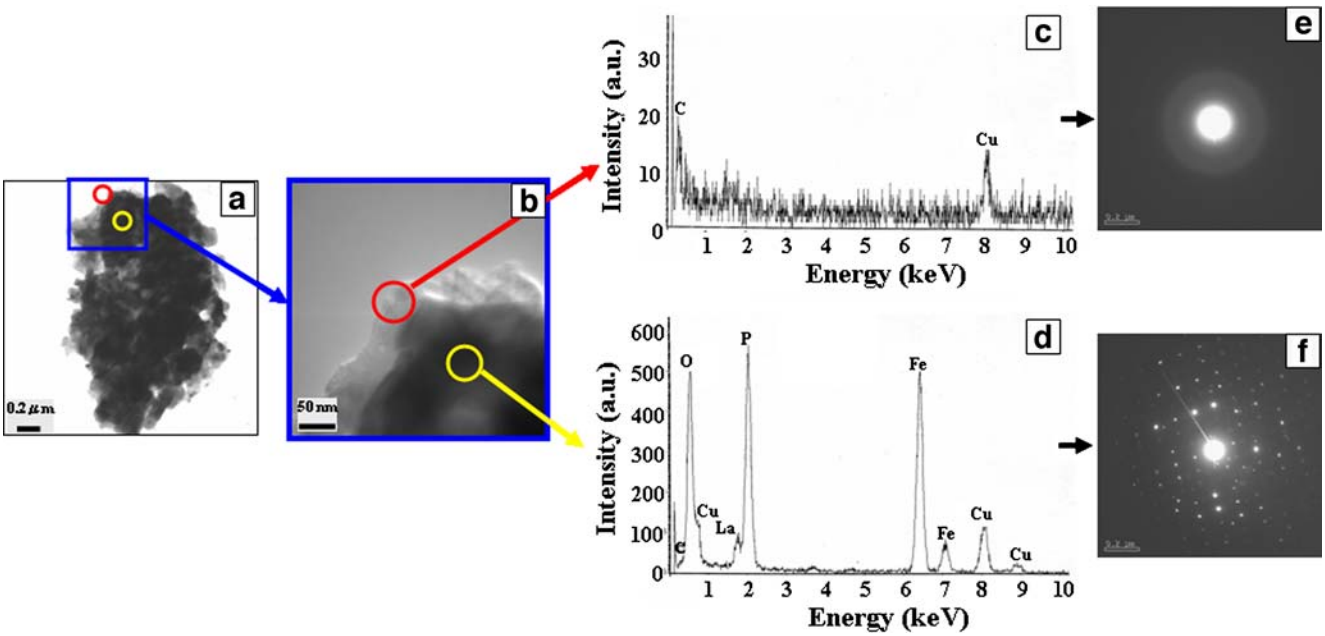

Fig. 4 **a**, **b** TEM images of $LiFe_{0.99}La_{0.01}PO_4/C$ powders; **c**, **d** EDS analysis for the particles; **e**, **f** SAED for the particles

Table 1 Conductivity and carbon content of samples

Material	Electronic conductivity (S cm^{-1})	Carbon content (wt%)	Initial discharge capacity (mAh g^{-1})	Synthesis condition
Pure $LiFePO_4$	5.88×10^{-6}	0.02	102	1.0 mol% La, 973 K, 10 h
30 wt% salicylic acid	1.94×10^{-3}	1.20	119	
40 wt% salicylic acid	2.82×10^{-3}	1.84	140	
50 wt% salicylic acid	3.06×10^{-4}	3.04	151	
60 wt% salicylic acid	3.43×10^{-4}	3.33	130	
70 wt% salicylic acid	3.77×10^{-4}	4.76	100	
0.1 mol. % La-doped	2.38×10^{-5}	2.28	140	973 K, 10 h, 50 wt% salicylic acid
0.5 mol% La-doped	2.92×10^{-5}	2.64	148	
1.0 mol% La-doped	3.06×10^{-4}	3.04	151	
1.5 mol% La-doped	5.25×10^{-4}	2.23	129	
2.0 mol% La-doped	9.25×10^{-4}	2.04	128	

of large graphene clusters in the very disordered carbon structure improved electronic conductivity of the carbon deposit. The graphitic carbon in the residual carbon coating layer can provide better electronic contact between $LiFePO_4$/C particles and improve their electronic conductivity and electrochemical performance.

The peak intensity ratios between 1,350 and 1,590 cm^{-1} can be calculated as R values (I_D/I_G), and are used to estimate the degree of disordering. These values indicate that the carbon can be pyrolyzed to form highly graphitized carbons with low I_D/I_G ratios and good electronic properties [33]. During pyrolysis of the organic acid precursor as the temperature was increased from 773 to 973 K, the minimum I_D/I_G ratio of $LiFe_{0.99}La_{0.01}PO_4$/C was 0.9398 at 873 K, revealing that some amounts of graphite-like or crystalline carbon were formed in the very disordered carbon web that wrapped around and connected the $LiFePO_4$ particles. TEM/SAED analysis in Fig. 4b and e shows that an amorphous nanometer-sized carbon coating layer was on the surface of La-doped $LiFePO_4$/C particles. The coating thickness was only a few nanometers, and it was too small to be analyzed by EDS. However, the presence of crystalline carbon in the $LiFePO_4$/C composite cannot be ruled out according to our recent work [34].

Electrochemical properties

The capacity and cyclability of $LiFePO_4$ and $LiFe_{1-x}La_xPO_4$/C electrodes were determined by galvanostatic charge/discharge testing at a 0.2 C-rate. A comparison of the discharge capacity of pure $LiFePO_4$ and its La-doped samples treated with various wt% salicylic acids is shown in Fig. 6. In the case of the pure $LiFePO_4$ sample, the first discharge capacity was only 104 mAh g^{-1} due to low electronic conductivity (see Table 1, 5.88×10^{-6} S cm^{-1}) and high electrochemical polarization (see Fig. 7). When $LiFe_{0.99}La_{0.01}PO_4$ was treated with various wt% salicylic acids, they all exhibited the same flat discharge plateau at about 3.4 V vs Li with slight voltage polarization, as shown in Fig. 7. The small polarization of the composite materials should be ascribed to high electronic

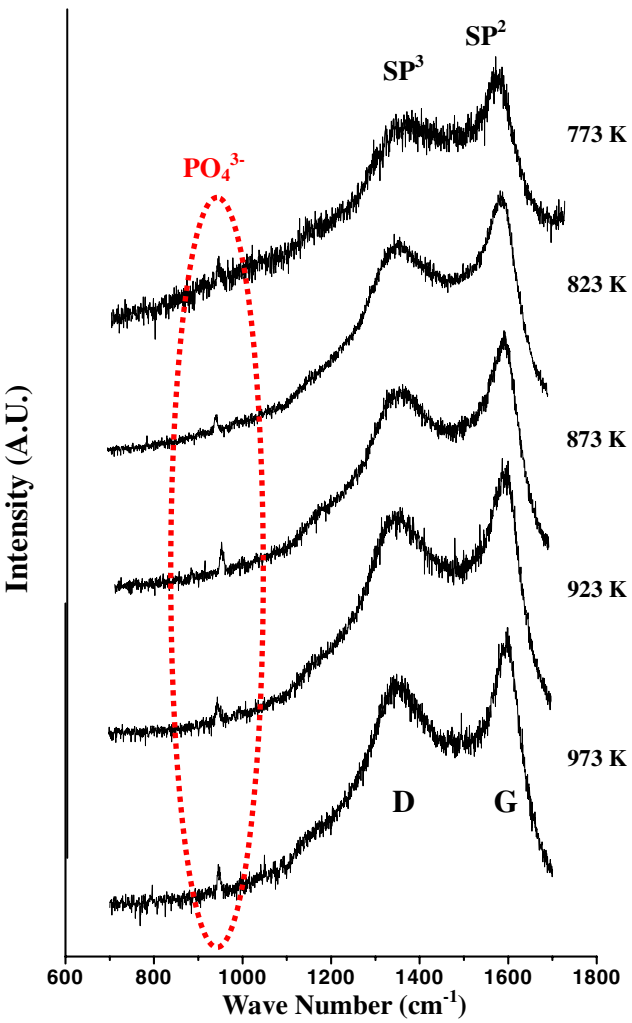

Fig. 5 Raman spectra of $LiFe_{0.99}La_{0.01}PO_4$/C materials prepared at various temperatures

Table 2 A Comparison of the conductivity, carbon content, and I_D/I_G ratio of samples

Temperature (K)	Electronic conductivity (S cm^{-1})	Carbon content (wt%)	Raman				Condition
			Peak (cm^{-1})		Intensity (A.U.)	I_D/I_G ratio	
773	1.18×10^{-4}	0.07	SP^3	1,374	1,467	0.9780	1 mol.% La, 10 h, 50 wt.% salicylic acid
			SP^2	1,600	1,500		
823	1.95×10^{-4}	1.07	SP^3	1,364	1,984	0.9475	
			SP^2	1,604	2,094		
873	3.06×10^{-4}	3.04	SP^3	1,369	1,516	0.9398	
			SP^2	1,600	1,613		
923	2.94×10^{-4}	3.50	SP^3	1,357	1,460	0.9624	
			SP^2	1,608	1,517		
973	2.59×10^{-4}	2.29	SP^3	1,358	1,374	0.9655	
			SP^2	1,606	1,423		

conductivity, indicating good electrochemical characteristics [4]. It is clear that $LiFe_{0.99}La_{0.01}PO_4$ treated with 50 wt% salicylic acid exhibited the best electrochemical performance. This is based on the combined results of discharge capacity and cycle number. To shorten cycling time, only the cycle number for curve (D) was completed based on 80% charge retention, and all other curves were estimated as indicated by the dotted lines in Figs. 6 and 8. The discharge capacity was correlated with carbon content, which was a suitable amount for the formation of a thin and uniform conductive layer. When carbon content increases, the ratio of the active material in the electrode decreases, leading to reduced capacity due to an increase in inactive carbon.

Figure 8 shows the discharge behavior of pure $LiFePO_4$ and $LiFePO_4$/C composites doped at various mol%. Figure 9 displays initial charge and discharge curves for pure $LiFePO_4$ and $LiFe_{1-x}La_xPO_4$/C electrode treated with 50 wt% salicylic acid. All $LiFe_{1-x}La_xPO_4$/C composites (x=0.1 to 2.0 mol%) show higher discharge capacity (over 130 mAh g^{-1}) and a flat discharge plateau at about 3.4 V vs Li with slightly less voltage polarization than pure $LiFePO_4$, as shown in Fig. 9. Among the doped samples, 1 mol% La-doped $LiFe_{1-x}La_xPO_4$/C demonstrated the best electrochemical performance with a first discharge capacity of 156 mAh g^{-1}. The doped $LiFePO_4$/C composites delivered higher capacity because its conductivity was improved as a result of increased p-type semiconductivity via the dopant effect as demonstrated in Table 1. However, even though the multivalent La^{3+} located in iron sites improved conductivity of the materials, Li^+ diffusion could be hindered if La^{3+} occupied too many iron sites and resulted in a decrease in discharge capacity. In addition, the carbon network of samples is an intrinsically inert material for Li^+ storage and the increasing carbon content would certainly lead to a capacity loss. Thus, the $Fe_{0.98}La_{0.02}PO_4$/C composite with the highest La-doped mol% did not exhibit the best electrochemical performance.

To evaluate the La doping effect on the cell performance of $LiFePO_4$/C composite material, we conducted different cycling tests. Figure 10 shows the discharge capacities of

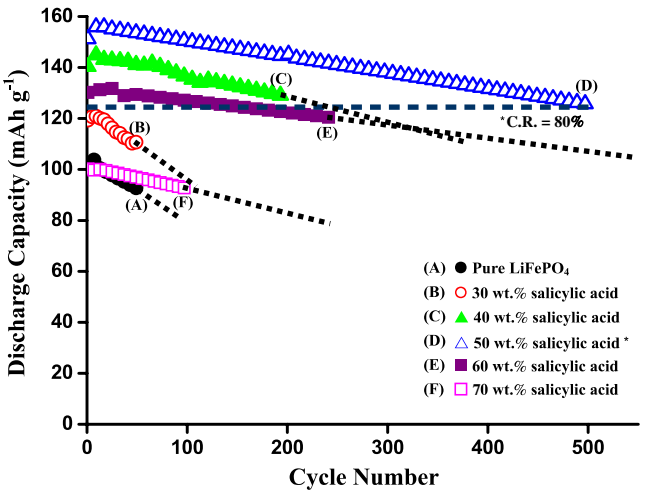

Fig. 6 Discharge capacity vs cycle number for pure $LiFePO_4$ and La-doped materials treated with various wt% salicylic acids. Charge/discharge: 4.0/2.8 V; 0.2 C-rate

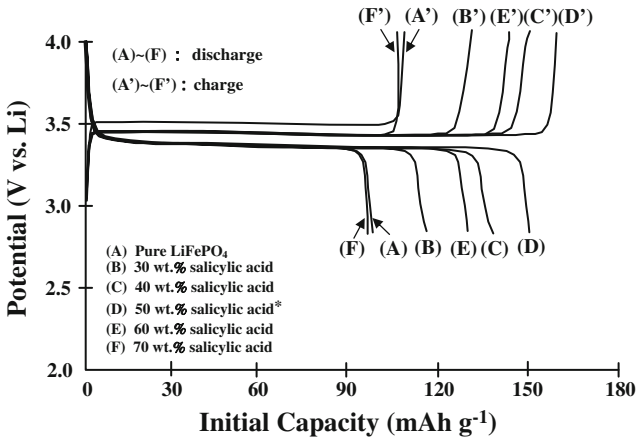

Fig. 7 Initial charge and discharge curves for pure $LiFePO_4$ and La-doped materials treated with various wt% salicylic acids. *(A)~(F)* Discharge, *(A')~(F')* charge

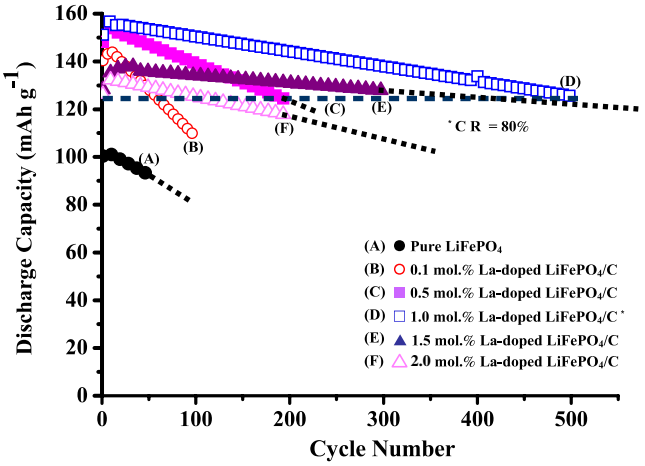

Fig. 8 Discharge capacity vs cycle number for pure $LiFePO_4$ and $LiFe_{1-x}La_xPO_4/C$ materials treated with 50 wt% salicylic acid. Charge/discharge: 4.0/2.8 V; 0.2 C-rate

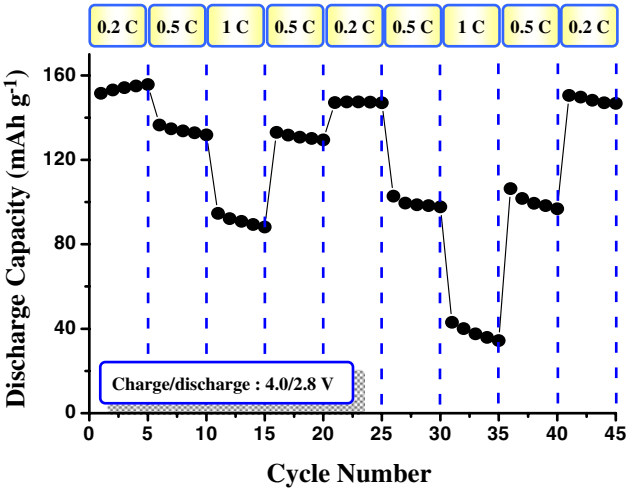

Fig. 10 The discharge behavior of a $LiFe_{0.99}La_{0.01}PO_4/C$ composite at various charge/discharge rates

$LiFe_{0.99}La_{0.01}PO_4/C$ electrodes observed in continuous cycling at rates varying from 0.2 to 1.0 C-rate between the voltage limits of 2.8~4.0 V. When the electrodes are charged and discharged at a high rate, the polarization of the electrodes is significantly high, so conductivity becomes an influential factor in determining the electrode kinetics of the electrochemical reaction. During the charge/discharge process, lithium intercalation/de-intercalation accompanied by an electron transfer reaction occurs both on the surface and inside the individual particles. Because the substitution of supervalent La^{3+} with Fe^{2+} in $LiFePO_4$ crystals improves the bulk conductivity, the electron transfer reaction would occur faster in La-doped $LiFePO_4/C$ than in pure $LiFePO_4$. It is important that a proper La doping level should be optimized to achieve a good cell performance.

The improvement in electrochemical properties of La-doped $LiFePO_4/C$ composites can be attributed to both La doping and carbon coating. These two methods are equally important. The non-lattice doping with carbon can increase the surface electronic conduction between particles, which does not represent the "true" conductivity of $LiFePO_4$ material. On the other hand, the lattice doping with lanthanum cation can intrinsically improve the "bulk" electronic conductivity of single $LiFePO_4$ particles by inducing increased p-type semiconductivity [24]. It is noteworthy that the improvement in electrochemical properties of La-doped $LiFePO_4/C$ composites did not depend solely on its carbon content. The mechanisms of how both carbon coating and metal doping affects electrochemical properties are not yet completely understood.

Cyclic voltammetry measurements were performed on $LiFe_{0.99}La_{0.01}PO_4/C$ electrodes to identify the characteristics of the redox reactions in Li-ion cells as shown in Fig. 11. A pair of redox reaction peaks appear in the CV curve. During

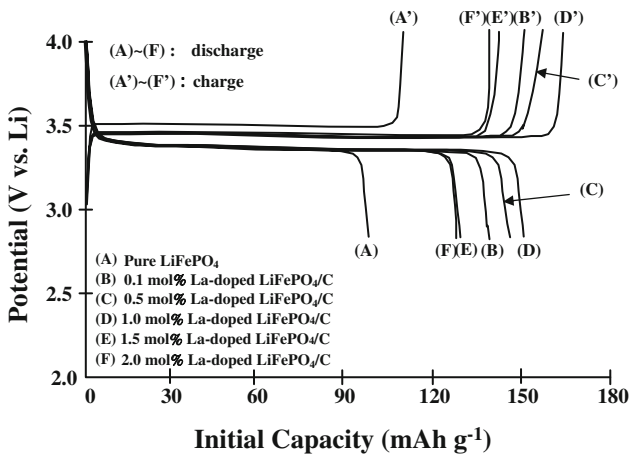

Fig. 9 Initial charge and discharge curves for pure $LiFePO_4$ and $LiFe_{1-x}La_xPO_4/C$ materials treated with 50 wt% salicylic acid. *(A)~(F)* Discharge, *(A')~(F')* charge

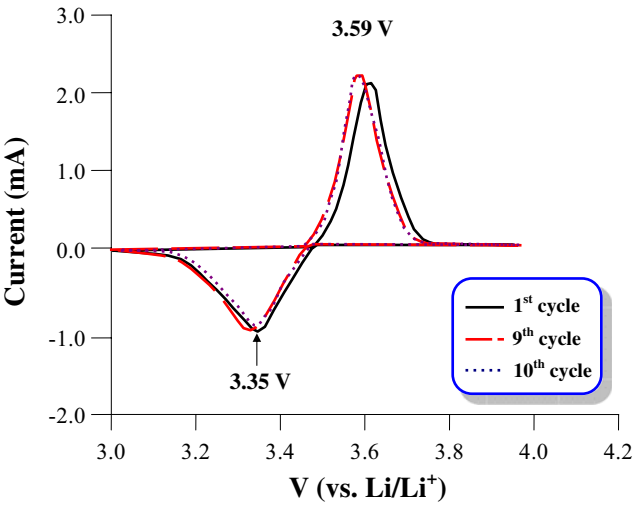

Fig. 11 CV profile of a $LiFe_{0.99}La_{0.01}PO_4/C$ composite at the scanning rate of 0.1 mV s^{-1}

an anodic sweep scanning from 3.0 to 4.0 V, a sharp oxidation peak at 3.59 V symbolizes the Li^+ de-intercalation from the $Li_xFe_{0.99}La_{0.01}PO_4/C$ structure. The corresponding reduction peak at 3.35 V indicates the Li^+ intercalation. The intense oxidation and reduction peaks indicated that Li^+ intercalation and de-intercalation occurred smoothly at the $Li_xFe_{0.99}La_{0.01}PO_4/C$ electrode. After ten cycles, the intensities of the redox peaks remained virtually unchanged, indicating good reversibility in the redox reaction. This is consistent with the long cycle life of our cathode material.

Conclusion

The physical and electrochemical properties of La-doped $LiFePO_4$ cathode materials synthesized via a high temperature solid-state method were systematically investigated. The La doping did not affect the structure of the cathode material, but considerably improved its capacity performance and cyclic stability. Among the materials studied, the $LiFe_{0.99}La_{0.01}PO_4/C$ composite demonstrated the best cell performance with a maximum discharge capacity of 156 mAh g^{-1} cycled between 2.8 and 4.0 V at a 0.2 C-rate, compared to 104 mAh g^{-1} for pure $LiFePO_4$. This composite electrode can sustain 497 cycles based on 80% charge retention. Such a significant improvement was mainly attributed to enhanced electronic conductivity (from 5.88×10^{-6} to 2.82×10^{-3} S cm^{-1}) and high Li^+ mobility in the doped samples.

Acknowledgement The authors thank Prof. W. H. Li (Department of Physics, National Central University) for his valuable suggestions and the use of Raman spectrometer.

References

1. Ozawa K (1994) Solid State Ion 69:212
2. Whittingham MS (2000) Solid State Ion 134:169
3. Armstrong AR, Bruce PG (1996) Nature 381:499
4. Padhi AK, Nanjundaswamy KS, Goodenough JB (1997) J Electrochem Soc 144:1188
5. Zane D, Carewska M, Scaccia S, Cardellini F, Prosini PP (2004) Electrochimica Acta 49:4259
6. Konstantinov K, Bewlay S, Wang GX, Lindsay M, Wang JZ, Liu HK, Dou SX, Ahn J-H (2004) Electrochim Acta 50:421
7. Gabersceka M, Dominkoa R, Belea M, Remskarb M, Hanzelb D, Jamnika J (2005) Solid State Ion 176:1801
8. Yang M-R, Teng T-H, Wu S-H (2006) J Power Sources 159:307
9. Nakamura T, Miwa Y, Tabuchi M, Yamada Y (2006) J Electrochem Soc 153:A1108
10. Park KS, Son JT, Chung HT, Kim SJ, Lee CH, Kang KT, Kim HG (2004) Solid State Comm 129:311
11. Gabrisch H, Wilcox JD, Doeff MM (2006) Electrochem Solid-State Lett 9:A360
12. Barker J, Saidi MY, Swoyer JL (2003) Electrochem Solid-State Lett 6(3):A53–A55
13. Salah AA, Mauger A, Julien CM, Gendron F (2006) Materials Science and Engineering B 129:232
14. Dong Q, Liu S, Zheng M, Zhan Y, Sun S, Lin Z (2006) Abstract 111, 209th ECS Meeting, May 7–12, Denver, Colorado
15. Eftekhari A (2004) J Electrochem Soc 151:A1456
16. Dominko R, Gaberscek M, Drofenik J, Bele M, Pejovnik S, Jamnik J (2003) J Power Sources 119–121:770
17. Zhang SS, Allen JL, Xu K, Jow TR (2005) J Power Sources 147:234–240
18. Xu Y, Lu Y, Yan L, Yang Z, Yang R (2006) J Power Sources 160:570
19. Herle PS, Ellis B, Coombs N, Nazar LF (2004) Nature mater 3:147
20. Chung SY, Blocking JT, Chiang YM (2002) Nature Mater 2:123
21. Ni JF, Zhou HH, Chen JT, Zhang XX (2005) Mater Lett 59:2361
22. Abbate M, Lala SM, Montoro LA, Rosolen JM (2005) Electrochem Solid-State Lett 8:A288
23. Wang GX, Bewlay S, Yao J, Ahn JH, Dou SX, Liu HK (2004) Electrochem Solid-State Lett 7:A503
24. Chung SY, Bloking J, Chiang YM (2002) Nat Mater 1:123
25. Herle PS, Ellis B, Coombs N, Nazar LF (2004) Nat Mater 3:147
26. Cullity BD, Stock SR, Elements of X-ray Diffraction (2001) Prentice Hall Publishers, New Jersey, USA, 3rd, Ch 5.2
27. Chen Z, Dahn JR (2002) J Electrochem 8:450
28. Zhang Z, Fouchard D, Rea JR (1998) J Power Sources 70:16
29. Ravet N, Abouimrane A, Amand M (2003) Nat Matters 2:702
30. Burba CM, Frech R (2004) J Electrochem Soc 151:A1032
31. Doeff MM, Hu Y, McLarnon F, Kostecki R (2003) Electrochem Solid-State Lett 6:A207
32. Hu Y, Doeff MM, Kostecki R, Finones R (2004) J Electrochem Soc 151:A1279
33. Doeff MM, Hu Y, McLarnon F, Kostecki R (2003) Electrochem. Solid State Lett 6:A207
34. Fey GTK, Lu TL (2008) J Power Sources 178:807